Low-frequency negative capacitance in $La_{0.8}Sr_{0.2}MnO_3$/Nb-doped $SrTiO_3$ heterojunction

C. C. Wang, G. Z. Liu, M. He, and H. B. Lu[a)]
Beijing National Laboratory for Condensed Matter Physics, Institute of Physics, Chinese Academy of Sciences, Beijing 100080, People's Republic of China

(Received 25 November 2007; accepted 13 January 2008; published online 7 February 2008)

Low-frequency ($100\ \text{Hz} \leqslant f \leqslant 1\ \text{MHz}$) dielectric properties of $La_{0.8}Sr_{0.2}MnO_3$/Nb-doped $SrTiO_3$ heterojunctions were investigated in detail at room temperature. Negative capacitance was observed at low frequencies under positive dc biases. This phenomenon was found to result from the combinational contributions from the Maxwell–Wagner interfacial relaxation and the dipolar relaxation related to detrapped carriers which give rise to inductive effect under an applied electric field. © *2008 American Institute of Physics*. [DOI: 10.1063/1.2840195]

Recently, manganite heterojunctions have attracted considerable attention due to their potential applications in spintronics,[1] hence, lots of research interest has been focused on the rectifying properties of magnetic diodes for the purpose of developing oxide electronics.[2–6] On the other hand, this kind of junction also possesses plentiful physical meanings, such as positive colossal magnetoresistance,[7,8] resistive switching between two or multilevel resistance states,[9] and colossal electroresistance.[10] We herein report another amazing property, i.e., the low-frequency negative capacitance (NC) effects in $La_{0.8}Sr_{0.2}MnO_3$ (LSMO)/Nb-doped $SrTiO_3$ (SNTO) heterojunction.

NC phenomenon has been experimentally evidenced and analyzed recently in a variety of electronic devices, such as *p-n* junctions, Schottky diodes, metal-semiconductor structures, glass alloys, etc.[11–15] Phenomenologically, NC effects indicate that the current variation lags behind the voltage agitation. However, the microscopic physical mechanisms of the NC in different devices are obviously different and have been ascribed to, e.g., contact injection, interface states, charge trapping, space charge effect, minority-carrier injection, etc. NC effects reported here were found to be closely related to the delocalization of the trapped carriers in the interface between LSMO and SNTO layers. Under an applied electric field, the delocalized carriers hop between localized positions giving rise to the inductive effect. NC appears when the inductive effect surpasses the Maxwell–Wagner interfacial polarization.

Two LSMO/SNTO structures denoted as F1 and F2 were fabricated using a computer-controlled laser molecular-beam epitaxy technique[16] by depositing LSMO films on (001) $SrNb_xTi_{1-x}O_3$ substrates with the Nb doping level $x=0.07$ and 0.01, respectively. Details about the deposition conditions can be found elsewhere.[17] The thickness of LSMO is about 720 nm. Dielectric measurements were carried out at room temperature using an Agilent 4294A precision impedance analyzer in a frequency range varying from 100 Hz to 1 MHz. The ac measuring signal was 50 mV rms. A gold pad with an area of 1 mm^2 was sputtered on LSMO thin film as the top electrode and the bottom electrode was In film (1 mm^2) pressed on to the NSTO substrate. Current to voltage (*I-V*) curves were measured by Keithley 2400 voltage source. Positive bias (i.e., forward bias) is defined as the current flow from SNTO to LSMO.

Figure 1 shows the leakage currents of F1 and F2 measured with the LSMO/SNTO structures sandwiched between the top and bottom electrodes. The *I-V* curves exhibit suitable rectifying properties mimics the conventional feature of the *p-n* junction. This feature can be identified to be related to the LSMO/SNTO heterojunction because the *I-V* curves obtained with the two electrodes on LSMO film or SNTO substrate exhibit perfect linear behavior (lower inset) confirming the Ohmic contact between the films (substrates) and the electrodes. In fact, the hole-doped $La_{0.8}Sr_{0.2}MnO_3$ is a *p*-type semiconductor, while the Nb-doped $SrTiO_3$ is a typical *n*-type semiconductor. It is well known that the rectifying *I-V* characteristic of a *p-n* junction originates from the built-in field in the interface of the junction, which depends on the energy band bending dominated by the deference of Fermi level between the *p*- and *n*-type semiconductors. Compared with the result of F2, the enhanced rectifying *I-V* characteristic of F1 indicates that the Fermi level of the heavily doped SNTO substrate is increased. Furthermore, a careful examination reveals that the leakage current at the reverse

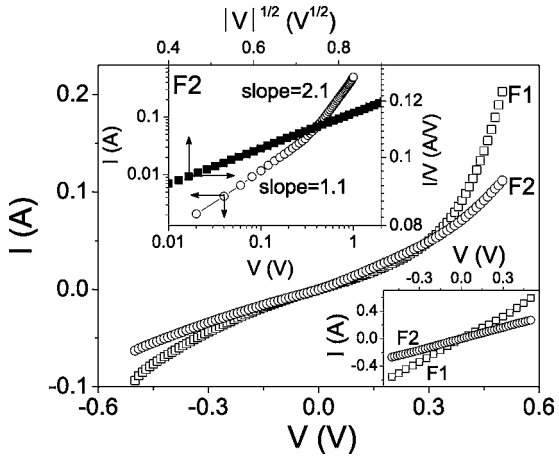

FIG. 1. Room temperature *I-V* curves for F1 and F2 measured with the LSMO/SNTO junctions sandwiched between the top and bottom electrodes. Lower inset: *I-V* curves for F1 and F2 measured with the two electrodes on the same side of the junction. Upper inset: Replots of the *I-V* curves for F2 using space charge limited current model for the forward bias and the Schottky emission model for the reverse bias voltages.

[a)]Author to whom correspondence should be addressed. Electronic mail: hblu@aphy.iphy.ac.cn.

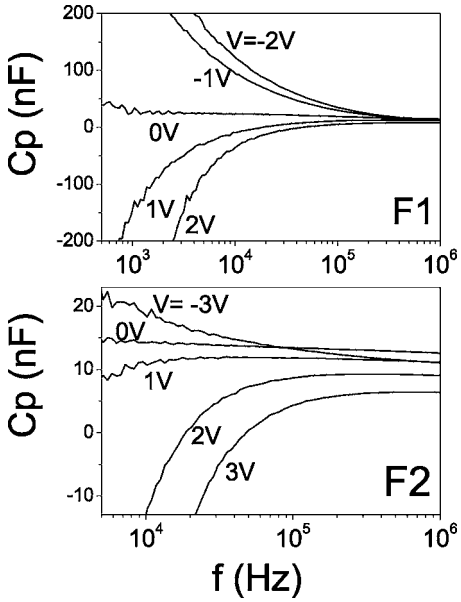

FIG. 2. Capacitance as a function of frequency for F1 and F2 at various bias voltages.

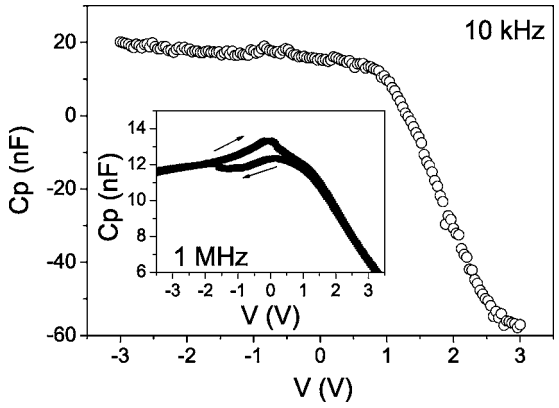

FIG. 3. Capacitance-voltage curve for F2 recorded at 10 kHz. Inset shows the capacitance-voltage curve for F2 at 1 MHz recorded with the bias sweeping upwards and then downwards.

bias voltages follows the Schottky emission model, i.e., $\log(I/V) \propto V^{1/2}$, as seen from the closed squares in the topper inset of Fig. 1. While at the forward bias voltages, the curve of $\log I \sim \log V$ (open circles in the topper inset of Fig. 1) shows a slope of 1.1 and 2.1 in the low- and high-bias ranges, respectively. This fact demonstrates that the leakage current obeys space charge limited current model in forward bias range, which indicates the interfaces of the *p-n* junctions contain a large number of localized defect states.

Figure 2 reports the frequency dependence of the measured capacitance of F1 and F2 under various dc biases (V). We note that the curves appear to achieve saturation at high frequencies. While at low frequencies, the capacitance is strongly dependent on both frequency and bias. The capacitance at negative biases is positive and decreases rapidly with the frequency featuring an interfacial polarization nature. The positive bias strongly suppresses the low-frequency upturn of capacitance, and when the positive bias is larger than a critical value V_C, NC effects can be observed in both films. It is clearly seen that V_C in F2 is larger than that in F1, implying that the NC effects are closely related to the *p-n* junction. Actually, NC effects occur at the low frequency range where the interfacial polarization dominates. There are three interfaces in the investigated films, i.e., Au/LSMO, *p-n* junction, and NSTO/In. The Ohmic contact between the films (substrates) and the electrodes let us conclude that the NC effects are undoubtedly due to the *p-n* junction.

Figure 3 displays the capacitance-voltage (C_p-V) result of F2 measured at a frequency $f=10$ kHz. The C_p-V curve features a behavior similar to that found in metal-oxide-semiconductor (MOS) device, i.e., C_p-V undergoes a translation from the accumulation region to the depletion or inversion region as the applied voltage sweeps from negative to positive values. This fact further convinces the point that NC effects are related to the *p-n* junction. Furthermore, for an ideal MOS device the above translation occurs at the voltage $V=0$. The offset of C_p-V curve with respect to the ideal MOS device usually results from the built-in electric field induced by localized charges.[18] The C_p-V curve of F2 shifts markedly to positive bias indicating that the NC effects found here are linked with the localized charges. A corroborating result convincing the existence of the localized charges is the hysteresis loop in C_p-V curve, as shown in the inset of the figure wherein a representative C_p-V loop measured at $f=1$ MHz was plotted. Generally, this kind of loop can be caused by ferroelectric polarization and trapped charges.[19] In the absence of ferroelectric material in the investigated films, the loop is, therefore, regarded as a proof of charge trapping in the films.

We now turn attention to the origin of the NC effects. Since the effects occur at low frequencies where the interfacial polarization dominates, a conceivable polarization is the Maxwell–Wagner relaxation due to the deference of conductivities and permittivities between LSMO and SNTO layers. The dielectric constant (capacitance) ε_M related to Maxwell–Wagner relaxation is given by[20]

$$\varepsilon_M \propto \Delta\varepsilon_M/[1+(\omega\tau_M)^2], \tag{1}$$

where $\omega=2\pi f$ is the angular frequency, τ_M is the relaxation time, and the polarization strength $\Delta\varepsilon_M=\varepsilon_s-\varepsilon_\infty$, in which ε_s and ε_∞ present the static and high-frequency dielectric constants, respectively. However, this relaxation gives rise to positive capacitance, which suggests that additional polarization, other than Maxwell–Wagner relaxation, is responsible for the NC effects. As already mentioned that the *p-n* junctions possess of a large number of localized defect states, it is, therefore, expected that part of the injected carriers from the electrode may be trapped by these states. It is important to point out that manganites are quite different from the conventional semiconductors owing to their strong coupling of the charge, lattice, spin, and orbital. In the depletion layer of LSMO, the rate of Mn^{3+}/Mn^{4+} increases dramatically. Since Mn^{3+} is a Jahn–Teller ion, strong distortion penetrating into the LSMO layer takes place. This greatly increases the number of localized defect states that causes more injected carriers reside in the localized states and contribute to the establishment of the built-in electric field. Under an applied field, some of the trapped carriers may detrap and can hop along the field direction. Because a certain time is needed for carriers to escape from their trap's states, this makes the current induced by the detrapping carriers lags behind the applied field, thereby causing the inductive effects. The hoping motions of the detrapped carriers not only gives rise to hopping conductivity but also creates dipolar effects.[21] The polariza-

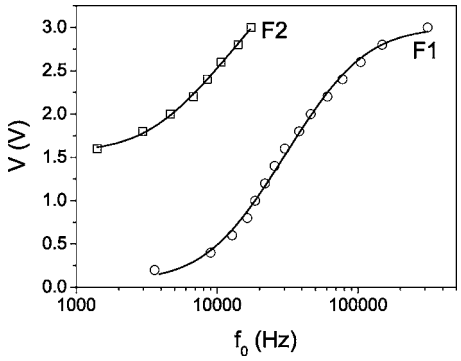

FIG. 4. Variation of the bias as a function of zero capacitance frequency. The solid curves are fitting results based on Eq. (5).

tion of the hopping detrapped carriers is proportional to the field activated carriers, the polarization strength $\Delta\varepsilon_D$ can be written as[22]

$$\Delta\varepsilon_D \propto \exp(-H/k_BT), \tag{2}$$

where k_B is the Boltzmann constant and H is the activation energy depending here on the applied field. Using the conventional double-well model,[23] one has the linear relationship between H and the applied bias V

$$H = H_0 - \alpha V, \tag{3}$$

where H_0 is the activation energy at $V=0$ and α is a constant. The negative dielectric constant (capacitance) ε_D associating with the detrapping carriers can be written as

$$\varepsilon_D \propto -\Delta\varepsilon_D/[1+(\omega\tau_D)^2], \tag{4}$$

where τ_D is the mean relaxation time of the detrapping carrier-induced dipole which is related to the inert of the carriers and varies with temperature following the Arrhenius law and therefore can be treated as voltage independent. The observed NC effects are dominated by the competitive contribution to polarization between the Maxwell–Wagner relaxation and the detrapping carrier-induced dipolar relaxation. Analytic results compared with the experimental data can be conduced at the frequency f_0 at which the measured capacitance $C_p(f_0)=0$, i.e., the two relaxations have equal contributions to the polarization. Based on Eqs. (1)–(4), we have

$$V = A - B \times \ln\{[1+(f_0\tau_M)^2]/[1+(f_0\tau_D)^2]\} \tag{5}$$

with $A=[H_0-k_BT\ln(1/\Delta/\varepsilon_M)]/\alpha$ and $B=k_BT/\alpha$ are temperature-dependent constants. Figure 4 presents such a comparison, from which we can see that the least-squares fittings based on Eq. (5) agree perfectly with the experimental data indicating the model used is suitable. The fittings yield the values of parameters τ_M and τ_D as 1.1×10^{-5} and 9.0×10^{-5} s in F1 and 1.8×10^{-5} and 2.0×10^{-4} s in F2. H_0 was determined to be 42 and 81 meV in F1 and F2, respectively. These values indicate that the dipolar polarization in F1 occurs easier than that in F2 as already seen.

In summary, the low-frequency NC effects in LSMO/SNTO heterojunctions have been investigated systematically. NC effects are linked with inductive effect, which was found to arise from the hopping motions of the detrapped carriers that also create dipolar effect. Our results indicate that the NC phenomenon depends on the collective contributions of the Maxwell–Wagner interfacial relaxation and dipolar relaxation to dielectric polarization.

The authors acknowledge the financial support from National Natural Science Foundation of China and National Key Basic Research Programmer of China. This work was also supported by China Postdoctoral Science Foundation.

[1] I. Žutić, J. Fabian, and S. D. Sarma, Rev. Mod. Phys. **76**, 323 (2004).
[2] P. L. Lang, Y. G. Zhao, B. Yang, X. L. Zhang, J. Li, P. Wang, and D. N. Zheng, Appl. Phys. Lett. **87**, 053502 (2005).
[3] F. X. Hu, J. Gao, J. R. Sun, and B. G. Shen, Appl. Phys. Lett. **83**, 1869 (2003).
[4] H. Tanaka, J. Zhang, and T. Kawai, Phys. Rev. Lett. **88**, 027204 (2002).
[5] C. M. Xiong, Y. G. Zhao, Z. H. Zhao, Z. O. Kou, Z. H. Cheng, H. F. Tian, H. X. Yang, and J. Q. Li, Appl. Phys. Lett. **89**, 143510 (2006).
[6] A. Sawa, T. Fujii, M. Kawasaki, and Y. Tokura, Appl. Phys. Lett. **86**, 112508 (2005).
[7] H. B. Lu, G. Z. Yang, Z. H. Chen, S. Y. Dai, Y. L. Zhou, K. J. Jin, B. L. Cheng, M. He, L. F. Liu, H. Z. Guo, Y. Y. Fei, W. F. Xiang, and L. Yan, Appl. Phys. Lett. **84**, 5007 (2004).
[8] K. J. Jin, H. B. Lu, Q. L. Zhou, K. Zhao, B. L. Cheng, Z. H. Chen, Y. L. Zhou, and G. Z. Yang, Phys. Rev. B **71**, 184428 (2005).
[9] A. Sawa, T. Fujii, M. Kawasaki, and Y. Tokura, Appl. Phys. Lett. **85**, 4073 (2004).
[10] X. P. Zhang, B. T. Xie, Y. S. Xiao, B. Yang, P. L. Lang, and Y. G. Zhao, Appl. Phys. Lett. **87**, 072506 (2005).
[11] For example, F. Lemml and N. M. Johnson, Appl. Phys. Lett. **74**, 251 (1999); G. B. Parravicini, A. Stella, M. C. Ungureanu, and R. Kofman, *ibid.* **85**, 302 (2004); H. C. F. Martens, J. N. Huiberts, and P. W. M. Blom, *ibid.* **77**, 1852 (2000); L. S. C. Pingree, B. J. Scott, M. T. Russell, T. J. Marks, and M. C. Hersam, *ibid.* **86**, 073509 (2005); J. Shulman, S. Tsul, F. Chen, Y. Y. Xue, and C. W. Chu, *ibid.* **90**, 032902 (2007).
[12] M. Ershov, H. C. Liu, L. Li, M. Buchanan, Z. R. Wasilewski, and A. K. Jonscher, IEEE Trans. Electron Devices **45**, 2196 (1998).
[13] X. Wu, E. S. Yang, and H. L. Evans, J. Appl. Phys. **68**, 2845 (1990).
[14] H. H. P. Gommans, M. Kemerink, and R. A. J. Janssen, Phys. Rev. B **72**, 235204 (2005).
[15] N. A. Penin, Semiconductors **30**, 340 (1996).
[16] G. Z. Yang, H. B. Lu, F. Chen, T. Zhao, and Z. H. Chen, J. Cryst. Growth **227–228**, 929 (2001).
[17] H. B. Lu, S. Y. Dai, Z. H. Chen, Y. L. Zhou, B. L. Cheng, K. J. Jin, L. F. Liu, G. Z. Yang, and X. L. Ma, Appl. Phys. Lett. **86**, 032502 (2005).
[18] S. W. Wang, W. Lu, X. S. Chen, N. Dai, and X. C. Shen, Appl. Phys. Lett. **81**, 111 (2002).
[19] J. P. Han, S. M. Koo, C. A. Richter, and E. M. Vogel, Appl. Phys. Lett. **85**, 1439 (2004).
[20] A. F. Gibson, F. A. Kröger, and R. E. Burgess, *Progress in Semiconductors* (Heywood, London, 1960), Vol. 4, pp. 65–90.
[21] A. K. Jonscher, *Dielectric Relaxation in Solids* (Chelsea, London, 1983), pp. 47–251.
[22] I. G. Austin and N. F. Mott, Adv. Phys. **18**, 41 (1969).
[23] J. R. Jameson, W. Harrison, P. B. Griffin, and J. D. Plummer, Appl. Phys. Lett. **84**, 3489 (2004).